Opto-Electronic Advances

ISSN 2096-4579 CN 51-1781/TN

Light-induced enhancement of exciton transport in organic molecular crystal

Xiao-Ze Li, Shuting Dai, Hong-Hua Fang, Yiwen Ren, Yong Yuan, Jiawen Liu, Chenchen Zhang, Pu Wang, Fangxu Yang, Wenjing Tian, Bin Xu and Hong-Bo Sun

Citation: Li XZ, Dai ST, Fang HH, et al. Light-induced enhancement of exciton transport in organic molecular crystal. *Opto-Electron Adv* **8**, 240207(2025).

https://doi.org/10.29026/oea.2025.240207

Received: 7 September 2024; Accepted: 20 January 2025; Published online: 28 March 2025

Opto-Electronic Advances

Article

April 2025, Vol. 8, No. 4

DOI: 10.29026/oea.2025.240207 CSTR: 32247.14.oea.2025.240207

Light-induced enhancement of exciton transport in organic molecular crystal

Xiao-Ze Li[1†], Shuting Dai[2†], Hong-Hua Fang[1*], Yiwen Ren[3], Yong Yuan[1], Jiawen Liu[2], Chenchen Zhang[2], Pu Wang[4,5], Fangxu Yang[3], Wenjing Tian[2], Bin Xu[2*] and Hong-Bo Sun[1*]

Efficient exciton transport over long distances is crucial for organic optoelectronics. Despite efforts to improve the transport properties of organic semiconductors, the limited exciton diffusion remains a significant obstacle for light-harvesting applications. In this study, we observe phenomena where exciton transport is significantly enhanced by light irradiation in the organic molecular crystal of 2,2'-(2,5-bis(2,2-diphenylvinyl)-1,4-phenylene) dinaphthalene (BDVPN). The exciton transport in this material is improved, as evidenced by the increased diffusion coefficient from 10^{-3} $cm^2 \cdot s^{-1}$ to over 1 $cm^2 \cdot s^{-1}$ and a prolonged diffusion length from less than 50 nm to nearly 700 nm characterized by time-resolved photoluminescence microscopy (TPLM). Additionally, we confirmed the enhancement of charge transport capability under irradiation as additional evidence of improved transport properties of the material. These intriguing phenomena may be associated with the material's twisted molecular conformation and rotatable single bonds, which facilitate light-induced structural alterations conducive to efficient transport properties. Our work provides a novel insight into developing organic semiconductors with efficient exciton transport.

Keywords: organic semiconductor; enhanced transport properties; exciton diffusion; time-resolved photoluminescence microscopy

Li XZ, Dai ST, Fang HH et al. Light-induced enhancement of exciton transport in organic molecular crystal. *Opto-Electron Adv* **8**, 240207 (2025).

Introduction

Exciton transport in organic semiconductors is critical as it is the essential process for the operation of organic light-harvesting devices, such as solar cells and photodetectors[1,2]. Only when photogenerated excitons reach the charge separation interface can the energy carried by the excitons be utilized. However, the transport of excitons in organic semiconductors is often hindered by various factors, including strong exciton-phonon couplings, strong electron-hole Coulomb interactions, and weak van der Waals interactions among molecules. These factors cause the localization of exciton wavefunctions in

[1]State Key Laboratory of Precision Measurement Technology and Instruments, Department of Precision Instrument, Tsinghua University, Beijing 100084, China; [2]State Key Laboratory of Supramolecular Structure and Materials, College of Chemistry, Jilin University, Changchun 130012 China; [3]Tianjin Key Laboratory of Molecular Optoelectronic Sciences, Department of Chemistry, School of Science, Tianjin University & Collaborative Innovation Center of Chemical Science and Engineering, Tianjin 300072, China; [4]Beijing National Laboratory for Molecular Sciences, Key Laboratory of Organic Solids, Institute of Chemistry, Chinese Academy of Sciences, Beijing 100190, China; [5]School of Chemical Sciences, University of Chinese Academy of Sciences, Beijing 100049, China.

[†]These authors contributed equally to this work.

*Correspondence: HH Fang, E-mail: hfang@mail.tsinghua.edu.cn; B Xu, E-mail: xubin@jlu.edu.cn; HB Sun, E-mail: hbsun@tsinghua.edu.cn

Received: 7 September 2024; Accepted: 20 January 2025; Published online: 28 March 2025

organic semiconductors[3,4]. As a result, exciton transport is generally achieved through inefficient incoherent hopping via Förster resonance energy transfer. Organic semiconductors' corresponding diffusion coefficients and diffusion lengths are typically limited to below 10^{-2} cm^2/s and 50 nm, respectively[5–11]. These limitations inherently cap the performance of organic photovoltaic devices, which often require nanoscale bulk heterojunctions —where donors and acceptors are intricately mixed—to ensure that excitons need only traverse short distances to the charge separation interfaces. Unfortunately, this compromise exacts a toll on the devices' charge collection, stability, and reproducibility. Therefore, the quest for organic semiconductors that facilitate efficient exciton transport is urgent for developing the next generation of high-performance organic photovoltaic devices.

The key to unlocking the full potential of organic semiconductor devices lies in enhancing their transport properties. Over the past few decades, substantial research has been dedicated to this end, and recent years have witnessed several promising breakthroughs. For instance, coupling excitons to photons allows for the propagation of excitation energy in the form of polaritons at speeds approaching light[12–14]. However, this typically requires sophisticated structural design, and polaritons flow is also beyond the scope of exciton transport. Similarly, isolated self-assembled nanostructures have demonstrated remarkable efficiency in exciton transport[15–19], with reports of diffusion lengths reaching 4.4 μm in nanofibers[15], and diffusion coefficient as high as 6.4±0.2 $cm^2 \cdot s^{-1}$ in nanotubes[18]. Despite these advancements, the utility of these nanostructures in practical devices remains limited. Additionally, the reported high diffusion coefficients are often measured during the initial, ultrafast phase of exciton dynamics (within 15 picoseconds), which may not accurately reflect the true transport capabilities of excitons over their entire lifetime. While the exploitation of triplet excitons with their longer lifetimes has been reported to enhance diffusion lengths to the micron scale or beyond[20–22], the diffusion coefficient of triplet excitons is not significantly improved compared to singlet excitons. Thus, there is a critical need for organic semiconductors that can efficiently transport singlet excitons throughout their entire lifetime to be suitable for device applications.

Here, we have synthesized a molecular crystal featuring a twisted molecular structure. Through a post-processing step involving light irradiation, we have achieved a spectacular enhancement in the diffusion coefficient, elevating it by three orders of magnitude to a value of 1.45±0.19 $cm^2 \cdot s^{-1}$. This value is comparable to those in some inorganic semiconductors that exhibit efficient exciton transport, such as perovskite crystals and 2D materials (see Table S3)[23–25]. Concurrently, the diffusion length has been increased from less than 32 nm to 672 ± 44 nm. We have systematically excluded the influence of water and oxygen on exciton transport during the irradiation process, attributing the marked improvement in transport properties to the structural modifications induced within the crystal lattice. Furthermore, we demonstrate enhanced charge transport upon irradiation, as evidenced by increased dark current from being undetectable to exceeding the sensitivity limit by an order of magnitude. These observations indicate a comprehensive enhancement in the material's transport properties. Finally, we discuss possible underlying mechanisms. The rotatable and twisted molecular structure lays the groundwork for structural changes upon irradiation. The formation of C–H···π and H···H interactions between intermolecular functional groups is instrumental in preserving the crystal's long-range order and reducing structural disorder. Consequently, the exciton behavior transitions from incoherent hopping to a more delocalized transport mechanism, conducive to improved performance in semiconductor devices. This work provides a novel perspective on preparing organic semiconductors with efficient transport properties, opening new avenues for their application in next-generation high-performance devices such as flexible organic photovoltaics, highly sensitive photodetectors, efficient organic light-emitting diodes (OLEDs), and advanced organic field-effect transistors (OFETs)[26–30]. These developments hold promise for transforming key areas including wearable electronics, energy harvesting systems, and environmentally sustainable technologies.

Method

Crystal growth method

1 mg BDVPN was added to a 20 mL glass bottle and dissolved in dichloromethane, followed by a slow addition of petroleum ether along the inner surface of the bottle (dichloromethane/petroleum ether: V/V=1/2). The entire system was placed in a stable location at room temperature, shielded from direct light. After the slow

evaporation progress, needle-like crystals exhibiting cyan emission were selected for subsequent analysis and characterization.

Transient photoluminescence-microscopy (TPLM)

The exciton diffusion was characterized by the home-built TPLM. It is similar to a PL confocal microscope but with some modifications. A 405 nm femtosecond pulse laser generated through the second harmonic generation of an 810 nm femtosecond laser (MaiTai) with a repetition rate of 80 MHz was focused onto the surface of the sample using an objective lens (Olympus, 100X, Apo, 0.95 numerical aperture), generating a Gaussian-distribution spot close to the diffraction limit. Unless otherwise stated, all measurements were done with a low average incident power of ~5 nW. Then the PL from the photoexcitation densities was collected by the same objective. The resulting collimated beam passes through a notch filter (405 nm, Edmund) to remove the reflected and scattered excitation light. Then the PL beam was focused to an image plane by an achromatic lens (f = 200 mm, Thorlabs), resulting in a total magnification of 111. A single-photon detecting avalanche photodiode (APD) (MPD PDM Series 20 μm) that is attached to the timing electronics (PicoQuant PicoHarp 300) was mounted on a two-axis motor stage (Thorlabs) at the image plane. The time evolution of the PL map was then recorded by scanning the time-resolved APD.

Spectrally resolved PL

The measurement is based on the same excitation light path of the home-built TPLM. The PL signal was led out of the TPLM system, and the spectra were recorded by Andor Kymera 193i.

Time-resolved PL decay

The measurement of time-resolved PL decay was based on the same excitation light path of the home-built TPLM, but the PL signal was collected by leading it out of the TPLM system and sending it to another APD (MPD PDM Series 20 μm) that is also attached to the timing electronics (PicoQuant PicoHarp 300). The difference with the APD used in TPLM is that the PL signal is focused within the APD photosensitive area through a lens with a short focal length. This configuration enables the APD to capture the complete PL signals accurately, thereby preventing errors in PL lifetime characterization.

UV-vis measurements

A Shimadzu UV-2700 spectrophotometer was employed to measure the UV-vis absorption spectra. The sample for the measurement was prepared by gently grinding BDVPN crystals into microcrystals and smearing them onto the quartz slice.

Electrical measurement

Au with a thickness of 120 nm was deposited by vapor deposition on top of SiO_2/Si that had been pre-modified with octadecyltrichlorosilane (OTS). Subsequently, the Au was mechanically transferred to the sample using a probe and adhered to the sample. The dark current was measured using a Keithley 4200 SCS in an ambient environment and at room temperature.

Results and discussion

Needle-like crystals with cyan emission (Fig. 1(b)) were obtained via the slow evaporation of BDVPN molecules (Fig. 1(a)) in a mixed solvent comprising dichloromethane and petroleum ether (V/V=1:2). The molecular structure and packing mode (Fig. 1(c)) were characterized by single-crystal X-ray diffraction (SCXRD) measurements (see Section 5, Supplementary information). The BDVPN crystals exhibit a broad photoluminescence (PL) spectrum with a peak wavelength at 484 nm and a full width at half maximum of 78 nm, as depicted in Fig. 1(d). Additionally, as illustrated in Fig. 1(e), the PL transient measurement reveals a single-exponential decay with a lifetime of 1.9 ns, indicative of highly efficient radiative recombination of singlet excitons. Unless otherwise specified, all PL signals were detected under low-power excitation (5 nW) to avoid potential high-order recombination processes that might occur under high-power excitation. Notably, the crystal edges exhibit intense emission under UV illumination (Fig. 1(b)), a characteristic indicative of a significant optical waveguiding effect. This suggests that the crystal features a well-suited geometric waveguide structure, highly ordered molecular alignment, and low optical loss. These characteristics provide an ideal optical cavity for applications such as low-threshold amplified spontaneous emission[31,32].

Exciton diffusion was characterized using Time-resolved PL Microscopy (TPLM), a powerful tool that has been extensively employed in a variety of semiconductors exhibiting strong PL emission, including molecular crystals[20], perovskites[33–35], and 2D materials[36–38]. In our

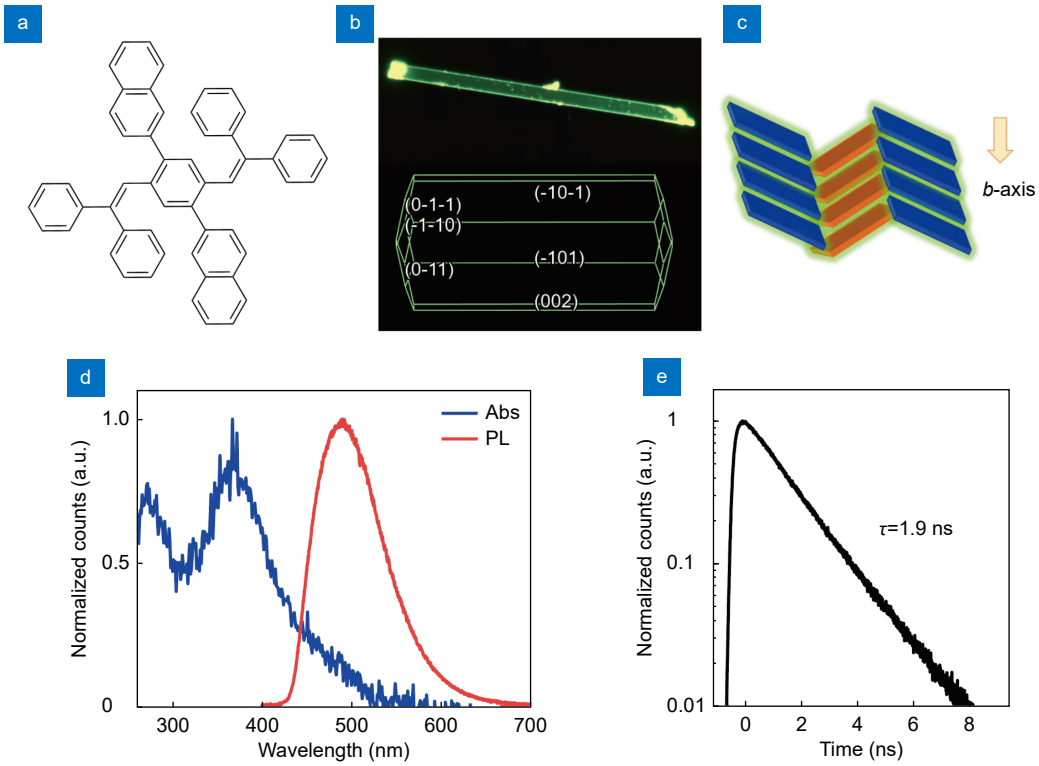

Fig. 1 | Crystal geometries and basic optical properties. (**a**) Chemical structure. (**b**) Optical microscope image of a BDVPN crystal under UV light (365 nm) (up) and schematic growth morphology of the crystal (down). (**c**) Schematic diagram of molecular packing viewed from *a*-axis. BDVPN molecules present herringbone packing mode and are aligned layer by layer along the *b*-axis (long axis of the crystal). (**d**) UV-vis and PL spectra, and (**e**) time-resolved PL of the BDVPN crystal.

experiment, a 405 nm fs laser (5 nW) was focused on a spot close to the diffraction limit at the surface of a BDVPN crystal, and the photogenerated excitons recombined radiatively while diffusing outward from the initial position. A single-photon detector avalanche photodiode (APD) that was connected to the Time-Correlated Single Photon Counting (TCSPC) module was positioned at the confocal image plane (Fig. 2(a)). Using the scanning APD (Fig. 2(b)), the exciton transport is visualized by tracking its spatially and time-resolved PL emission because PL intensity is proportional to the exciton density at low excitation. The measurement result of the intrinsic BDVPN crystal is presented in the left panel of Fig. 2(c), where the PL intensity is normalized at each time slice to display the diffusion process. The negligible broadening of PL width indicates limited exciton diffusion, a common trait in organic crystals. Subsequently, the sample was taken out from TPLM and underwent exposure to a collimated strip-shaped 405 nm continuous-wave (CW) laser (4 W·cm^{-2}) for some time (middle panel of Fig. 2(c)). Surprisingly, after undergoing irradiation treatment for about 45 minutes, the enhancement in exciton diffusion is visible, as evidenced by the gradual broadening of the PL width in the right panel of Fig. 2(c).

To quantify relevant diffusion parameters, *MSD* model was applied[39]:

$$MSD = \sigma_{\rm int}^2(t) - \sigma_{\rm int}^2(0) = 2Dt + MSD_{\rm offset}\ ,$$

where $\sigma_{\rm int}(t)$ represents the width of Gaussian exciton distribution, *MSD* is mean-squared displacement, which grows linearly over time. The diffusion coefficient (D) is proportional to the slope, while $MSD_{\rm offset}$ is a constant to accommodate the fitting error. Figure 2(d) displays the temporal evolution of MSD before and after irradiation treatment. Before irradiation treatment, a diffusion coefficient of 0.0030±0.0036 cm^2·s^{-1} was produced, which signified the intrinsically weak exciton diffusion coefficient of the BDVPN crystal. As the error interval is smaller than the value, the actual diffusion coefficient should be less than the error interval, i.e., 0.0036 cm^2·s^{-1}, due to the limitations of the testing precision. Following a 10 minute irradiation treatment, the diffusion coefficient increased to 0.036±0.006 cm^2·s^{-1} and subsequently rose to 0.18±0.02 cm^2·s^{-1} after 45 minutes. As a result, the diffusion coefficient increased significantly by two orders

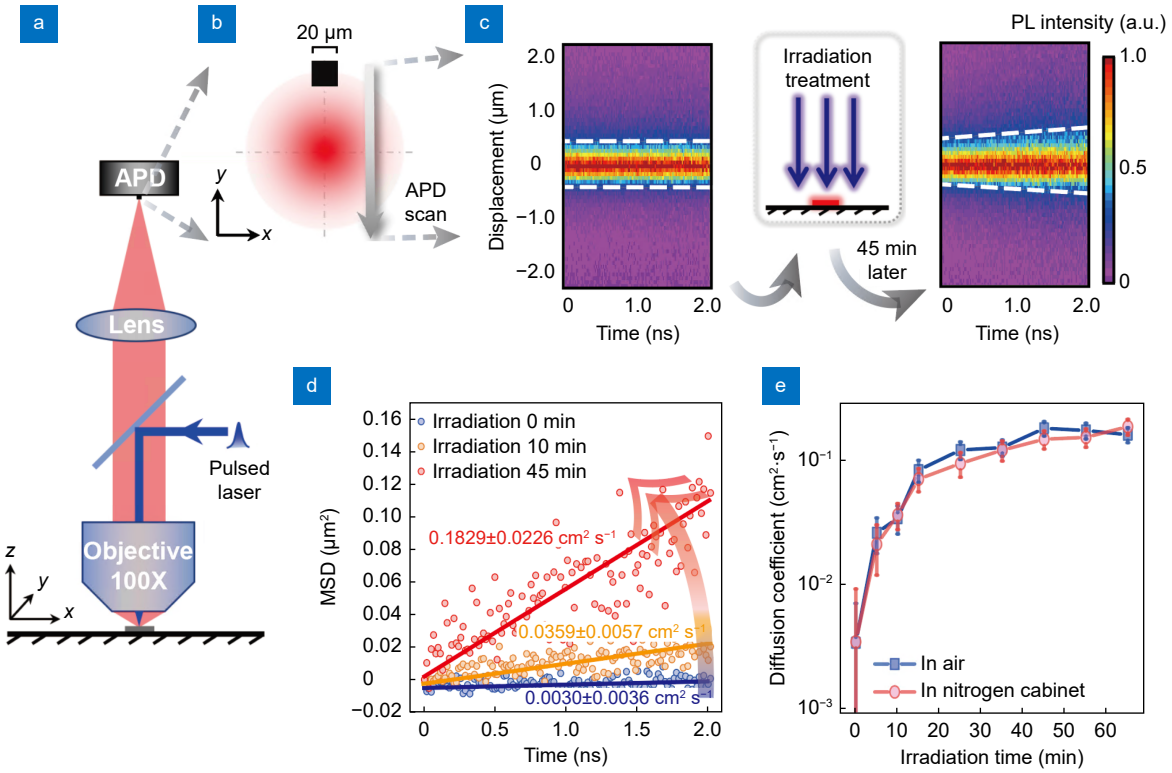

Fig. 2 | Irradiation-induced exciton diffusion enhancing and the roles of oxygen and water. (**a**) Schematic of the home-built TPLM. The PL signal is magnified at the image plane, as shown in (**b**), and the time-resolved APD is scanned across the PL spot to generate a spatial-temporal map of PL intensity. (**c**) The spatial-temporal PL intensity map of a BDVPN crystal before and after irradiation treatment by a collimated strip-shaped 405 nm CW laser (4 W cm^{-2}). (**d**) The measured *MSD* over time of the BDVPN crystal after being irradiated for 0 minutes (before irradiation), 10 minutes, 45 minutes. The solid lines show the results of linear fit, and resulting three diffusion coefficients of 0.0030±0.0036 cm^2·s^{-1}, 0.036±0.006 cm^2·s^{-1}, and 0.18±0.02 cm^2·s^{-1}. (**e**) The evolution of exciton diffusion coefficient of two BDVPN crystals under irradiation, where one crystal was exposed to ambient air and the other to a nitrogen environment.

of magnitude, surpassing 0.1 cm^2·s^{-1} within one hour of irradiation. Notably, when employing TPLM for exciton diffusion testing, we avoided the potential effects of fs laser irradiation at a fixed position by programmatically scanning the piezoelectric displacement stage. Additionally, the time range of the *MSD* used to extract diffusion coefficients is 2 ns, covering the entire duration of the exciton's lifetime. Therefore, the diffusion coefficient obtained reflects the exciton's transport capacity throughout its lifetime, not solely during the ultrafast initial stages.

At this point, the question arises: why is the exciton diffusion greatly enhanced? One plausible explanation is the involvement of oxygen and water, as previous studies have suggested that light can facilitate the entry of water and oxygen into materials, leading to the production of reactive species[40–42]. These species can alter the semiconductor's molecular motif or electronic state, potentially changing exciton transport properties. To exclude the impact of water and oxygen on the exciton diffusion under irradiation, we performed the irradiation treatment in air (Sample S1) and nitrogen environment (Sample S1-1), respectively. Sample S1-1 was obtained by cutting sample S1 to minimize potential discrepancies. Figure 2(e) illustrates the diffusion coefficient as a function of irradiation time, for one is in ambient air and the other is in the nitrogen cabinet. The diffusion coefficient increases with irradiation time, with similar trends and values, suggesting that water and oxygen in the air did not play a role in enhancing exciton diffusion. Additionally, we conducted a control experiment in a vacuum environment, further confirming that the observed enhancement of exciton transport under light irradiation is independent of environmental factors (see Section 8, Supplementary information).

To further investigate the extent of light-induced enhancement of exciton diffusion and its underlying mechanism. We extended the duration of irradiation in the nitrogen cabinet and periodically measured the exciton diffusion parameters and PL characteristics. Throughout

more than 100 hours of irradiation, a continuous enhancement in the exciton diffusion was noted (Fig. 3(a)). The enhancement of the exciton diffusion coefficient can be categorized into two stages. In the first stage, the diffusion coefficient increased from ~10^{-3} $cm^2 \cdot s^{-1}$ to ~0.1 $cm^2 \cdot s^{-1}$ within the first hour, corresponding to the red dotted line in Fig. 2(e). This was a rapid process during which the diffusion coefficient increased efficiently. In the second stage, the diffusion coefficient increased gradually in the next hundred hours, finally exceeding 1 $cm^2 \cdot s^{-1}$. This process entailed a prolonged duration during which the diffusion coefficient gradually reached saturation. Similar results were verified on other samples (see Section 2, Supplementary information), and prolonged irradiation didn't lead to a further increase but decreased diffusion coefficient due to degradation due to excessive irradiation (Fig. S2). Additionally, we show that the irradiation conditions that enhance exciton diffusion are not limited to CW laser; the irradiation of pulsed femtosecond laser and incoherent LED also increases the diffusion coefficient of BDVPN crystals, and the efficiency depends on the amount of irradiation absorbed by the crystal (see Section 3, Supplementary information). Simultaneously, we demonstrate that in tests utilizing TPLM, low-power (5 nW) femtosecond excitation laser irradiation does not impact the exciton diffusion properties of the crystal (Fig. S3(b)), particularly when employing a method of scanning displacement stage. So, the validity of the data results is ensured. In investigating the stability of the diffusion-enhanced state, we found that enhanced exciton diffusion represents a relatively stable state, with a diffusion coefficient exceeding 0.1 $cm^2 \cdot s^{-1}$ being sustained for at least several months (see Section 4, Supplementary information).

To analyze irradiation-induced changes in PL emission properties, we performed measurements of PL transient and spectra. The exciton lifetime, as determined by PL transients (see Fig. S11 for original data), exhibits a slight decrease as the irradiation time increases (blue dotted line in Fig. 3(c)). The diffusion lengths, calculated using the formula $L_D = \sqrt{2D\tau}$, increase significantly from around 30 nm to approaching 700 nm (red dotted

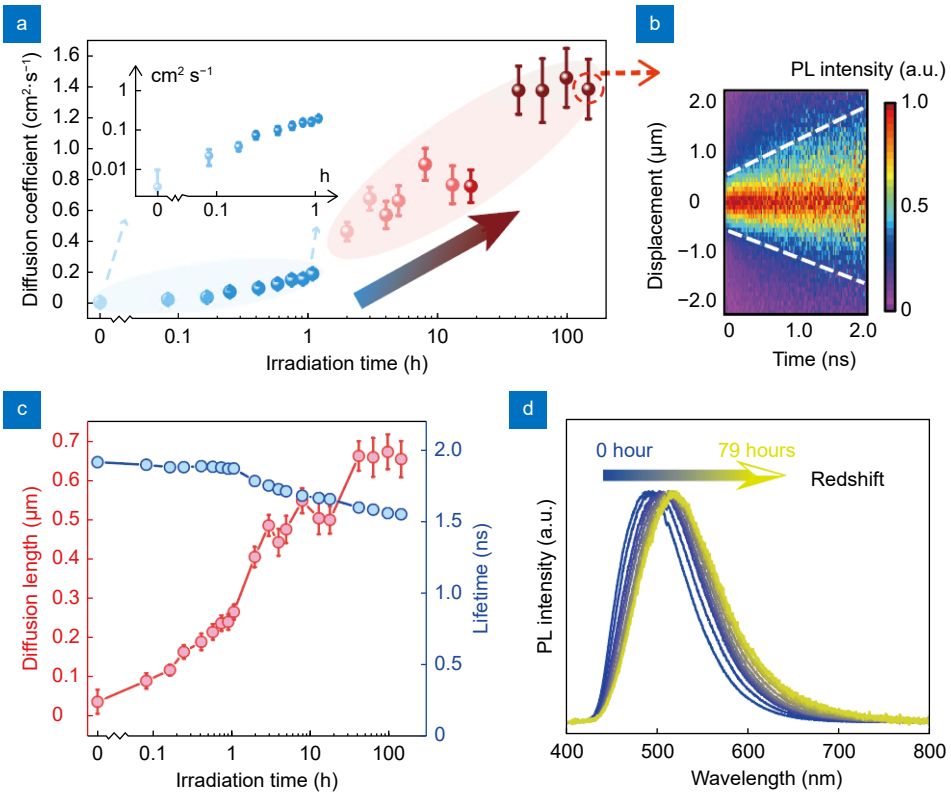

Fig. 3 | Impact of long period irradiation in nitrogen cabinet on diffusion parameters and PL properties. (**a**) The evolution of exciton diffusion coefficient after irradiation. The values are statistics results, each taken from several tests (see section SI1, Supplementary information). The inset shows the data corresponding to the first stages (blue dashed area) under logarithmic coordinates. (**b**) The fast broadening of PL emission over time for the BDVPN crystal irradiated for 145 hours. Compared with Fig. 2(c), the enhancement in exciton diffusion was visualized. (**c**) The evolution of exciton lifetime and diffusion length after irradiation. (**d**) Redshift of PL spectra with irradiation time.

line in Fig. 3(c)), surpassing most reported results for organic semiconductors (see Table S3)[5,43,44]. Meanwhile, we analyzed the PL spectra over tens of hours of irradiation, observing a consistent red shift throughout the process (Fig. 3(d)). Hence, within a nitrogen cabinet that is shielded from moisture and oxygen, the red shift in PL spectrum and the reduction in exciton lifetime due to irradiation indicate alterations in the crystal's structure, which fundamentally transformed the exciton transport properties of the crystal. Furthermore, the structural changes were confirmed through powder X-ray diffraction (PXRD) analyses of BDVPN microcrystals under irradiation (see Section 7, Supplementary information).

We are now exploring not only exciton diffusion but also charge transport, recognizing that these processes are characterized by different mechanisms. Exciton transport can be influenced by long-range dipole-dipole interactions between molecules, whereas charge transport predominantly relies on nearest-neighbor interactions tied to wavefunction overlap[45]. Despite these distinctions, both types of transport are crucial properties of materials and share similarities, such as being significantly impeded by disorder and enhanced by electronic coupling.

Given the BDVPN crystal's inherently low charge transport capabilities, directly characterizing its charge mobility through methods like Field effect transistor (FET) devices or space-charge-limited currents (SCLC) was challenging. To circumvent this, we characterized the changes in the dark current to assess the impact of irradiation on charge transport. The lateral-electrode device is shown in Fig. 4(a). A 405 nm CW laser with a maximum power output of 60 mW·cm^{-2} was utilized in this experiment. Figure 4(b) illustrates that, in the absence of irradiation, the dark current of the BDVPN crystal remained as low as 10^{-14} A, a value that scraped the lower limit of our detection equipment's sensitivity, indicative of highly inefficient charge transport. However, the current is increased after subjecting the sample to irradiation for approximately 2 hours. The experiment was conducted by irradiating the sample and then monitoring its dark current over time. The dark current increased to around 10^{-13} A after the irradiation. We also observed similar results in another device, and the improved charge transport properties persisted even after the device was kept in a dark and dry container for 18 hours (see Section 6, Supplementary information). Although BDVPN crystal did not exhibit efficient charge transport capabilities or endowment for application in electronics, the increased dark current did signify the holistic effect of irradiation on the material's transport properties, showcasing enhancements in both exciton diffusion and charge transport. These results highlight the potential benefits of irradiation in improving the transport performance of BDVPN crystal.

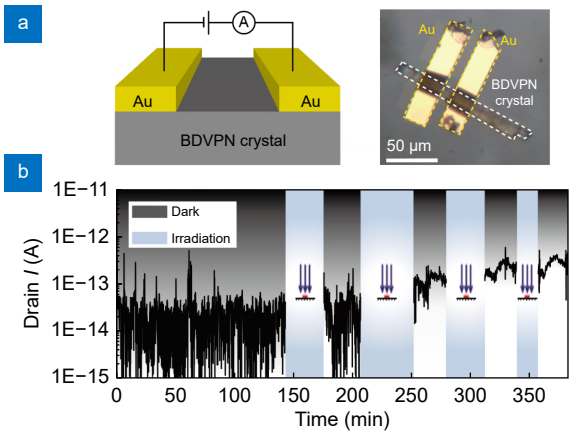

Fig. 4 | Enhancement of charge transport under irradiation. (**a**) Schematic and optical microscope images of the electrical device, two Au film electrodes were transferred to the crystal. (**b**) The evolution of dark current (at a 60 V applied voltage) of the BDVPN crystal over time before and after the irradiation treatment (405 nm CW laser, 60 mW ·cm^{-2}).

Since the properties of materials are always closely related to their structures, the enhancement of exciton diffusion combined with the changes in PL spectra and lifetime indicates changes in the crystal structures that facilitate improved exciton transport. To delineate the precise structural alterations that contributed to the observed results, we tried to characterize the crystal structure after the post-irradiation treatment. However, the uneven distribution of absorbed irradiation throughout the crystal, which leads to differences in properties and crystal structures, presented challenges for the single crystal diffraction test. Consequently, we resorted to a qualitative analysis based on the structure of the pristine crystal.

On the one hand, the molecular structure is susceptible to alteration. This is illustrated with Interaction region indicator (IRI) analysis, with the sign(λ_2)ρ function represented on IRI isosurfaces through color mapping, clearly illustrating the nature of the interaction regions. Figure 5(a) shows the standard coloring method and the corresponding explanation of sign(λ_2)ρ on IRI isosurfaces. The sign(λ_2) denotes the sign of the second largest

eigenvalue of Hessian of ρ, which distinguishes attractive and repulsive interactions. The regions with $\rho>0$ and thus large magnitude of sign(λ_2)ρ imply a relatively strong interaction, while areas with $\rho\approx0$ suggest very weak interatomic van der Waals interaction[46,47]. Therefore, the BDVPN crystal features van der Waals interactions (represented by green isosurfaces) between adjacent molecules, alongside strong repulsions (represented by red isosurfaces) between the hydrogen atoms on vinyl and naphthalene. This steric hindrance induces the butterfly wings and naphthalene to deviate from the central benzene, facilitated by the rotatable single bonds, thereby creating a highly twisted molecular structure (Fig. S5(a)). This rotatable and twisted molecular architecture lays the groundwork for structural modifications under irradiation.

On the other hand, specific molecular interaction is conducive to the maintenance of packing order. As shown in Fig. 5(b), despite adjacent molecules exhibiting a considerable intermolecular distance (the centroid distance between adjacent molecules' central benzene rings is 5.321 Å (1 Å = 0.1 nm), and the interface distance between central benzene rings is 4.698 Å, exceeding the typically defined π-π interaction distance[48]), the intrinsic crystals without irradiation treatment exhibit weak nearest-neighbor interactions that hinder efficient exciton and charge transport. However, the presence of C–H···π interactions (2.950 Å) between adjacent naphthalene rings and H···H interactions (2.331 Å) between the benzene rings of neighboring butterfly wings promotes the establishment of a long-range ordered packing mode. This can also be intuitively visualized through Hirshfeld surface analysis[47]. As shown in Fig. 5(c), the red spots indicate the presence of short contacts of C···H, while the white and blue regions represent the contacts close to van der Waals separation[49]. Notably, the minimal proportion of C···C contacts (0.6%) suggests a lack of π-π interactions between molecules. In contrast, the predominant

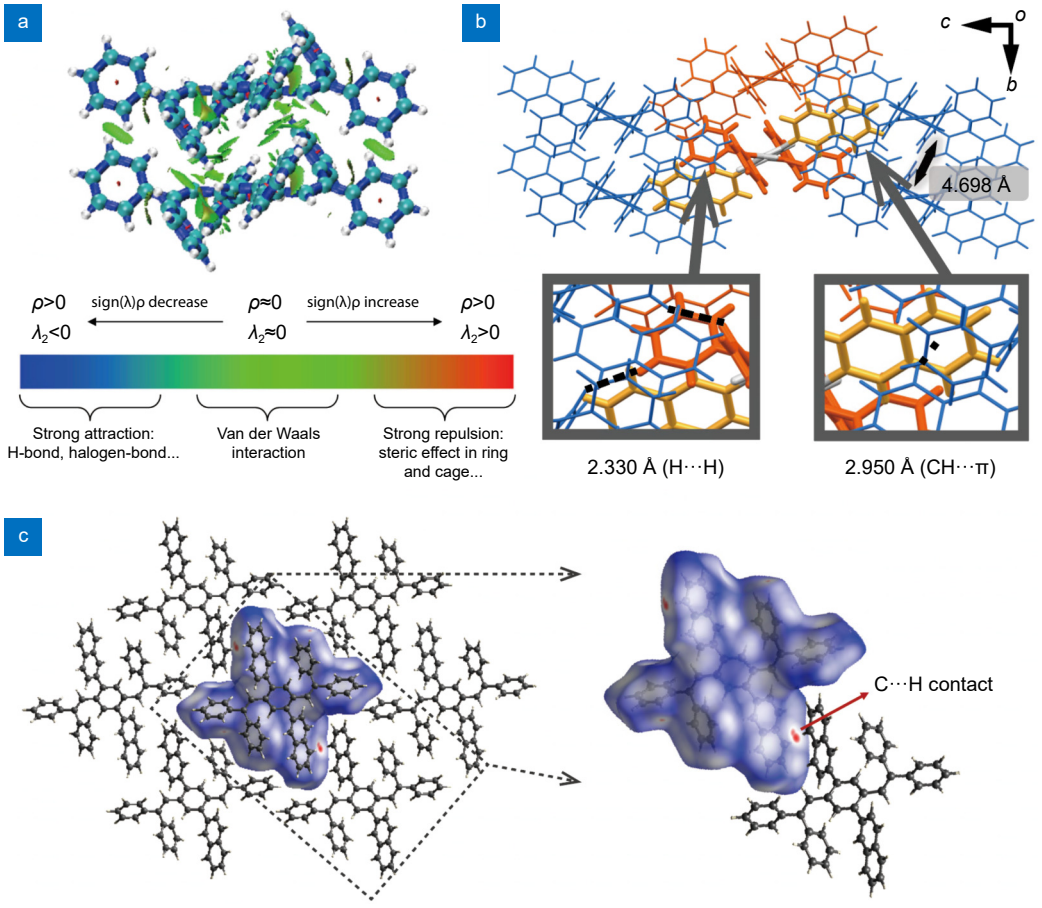

Fig. 5 | Intermolecular interactions analysis. (**a**) The isosurface map of the IRI for the BDVPN crystal. IRI analysis provides additional insights into intra- and intermolecular interactions through gradient isosurfaces and corresponding colors (determined by sign(λ_2)ρ values). (**b**) Molecular packing and intermolecular interactions of the crystal (The molecules drawn in orange and blue are the same conformation but arranged in different directions). (**c**) Hirshfeld surface of the BDVPN crystal. The red spots represent the close contact of C···H.

contributions of C···H (40.3%) and H···H (59.1%) contacts emphasize the roles of the C–H···π interactions and H···H interactions as the main driving forces in the molecular arrangement. Therefore, the crystal long-range order and low structure disorder are likely maintained throughout the process of irradiation-induced structural changes, which bias the crystal towards more efficient exciton transport. Nevertheless, further investigation is necessary to elucidate the precise structure after irradiation treatment and its correlation with the crystal's transport properties.

Regarding the mechanism of exciton diffusion in organic semiconductors, certain efficient exciton transport phenomena cannot be adequately explained by incoherent exciton hopping alone. Materials with lower disorder, reduced reorganization energy, and enhanced electronic coupling have facilitated higher degrees of exciton delocalization. These optimizations promote the transition of exciton transport from incoherent hopping towards a more coherent phase, giving rise to an intermediate regime in exciton transport between full localization and full delocalization stages[45]. Furthermore, coherent transport phenomena have been observed at certain low temperatures or within some natural light-harvesting complexes[50–52]. In the case of our BDVPN crystal, the diffusion coefficients as low as 10^{-3} $cm^2 \cdot s^{-1}$ in intrinsic samples without irradiation are characteristics of incoherent hopping, characterized by weak interaction and strong localization of excitons[5]. The dramatic increase to approximately 1 $cm^2 \cdot s^{-1}$ following irradiation signals a departure from the constraints of incoherent hopping, suggesting that exciton transport has entered a new regime[15]. Delocalization due to possibly increased electronic coupling, reduced reorganization energy, and a decrease in structural disorder within the crystal lattice must have played a significant role in the enhanced exciton transport process[3,15].

Conclusions

In summary, we have discovered an intriguing phenomenon of irradiation-induced enhancement in exciton transport. This enhancement elevated the intrinsic exciton diffusion coefficient from 10^{-3} $cm^2 \cdot s^{-1}$ to 1 $cm^2 \cdot s^{-1}$, and diffusion length from less than 32 nm to approaching 700 nm. We have ruled out the effects of oxygen and water on the enhanced exciton transport, and we speculate that the structural alterations of the crystal are responsible for the improved exciton diffusion. Moreover, we show evidence that irradiation not only boosts exciton diffusion capability but also enhances charge transport characteristics. The crystal's twisted and rotatable molecular structure appears to be intricately linked to structural changes induced by irradiation, with the intermolecular interaction, such as C–H···π interactions and H···H interactions, playing a pivotal role in preserving the packing order in the process of structural variation. This altered, ordered crystal structure is speculated to enhance the exciton delocalization, thereby orchestrating a significant shift from localized hopping to more efficient delocalized motion. Future inquiries are anticipated to thoroughly explore and characterize the post-irradiation structures, aiming to establish a direct correlation between these modifications and the material's augmented transport properties. Our research shines a spotlight on a fascinating phenomenon: the irradiation-induced enhancement of exciton diffusion within an organic molecular crystal (BDVPN), offering a promising route to overcome the historical challenge of inefficient exciton transport.

References

1. Menke SM, Luhman WA, Holmes RJ. Tailored exciton diffusion in organic photovoltaic cells for enhanced power conversion efficiency. *Nat Mater* **12**, 152–157 (2013).
2. Lu H, Chen K, Bobba RS et al. Simultaneously enhancing exciton/charge transport in organic solar cells by an organoboron additive. *Adv Mater* **34**, 2205926 (2022).
3. Sneyd AJ, Fukui T, Paleček D et al. Efficient energy transport in an organic semiconductor mediated by transient exciton delocalization. *Sci Adv* **7**, eabh4232 (2021).
4. Alvertis AM, Haber JB, Engel EA et al. Phonon-induced localization of excitons in molecular crystals from first principles. *Phys Rev Lett* **130**, 086401 (2023).
5. Mikhnenko OV, Blom PWM, Nguyen TQ. Exciton diffusion in organic semiconductors. *Energy Environ Sci* **8**, 1867–1888 (2015).
6. Menke SM, Holmes RJ. Exciton diffusion in organic photovoltaic cells. *Energy Environ Sci* **7**, 499–512 (2014).
7. Mikhnenko OV, Kuik M, Lin J et al. Trap-limited exciton diffusion in organic semiconductors. *Adv Mater* **26**, 1912–1917 (2014).
8. Hedley GJ, Ward AJ, Alekseev A et al. Determining the optimum morphology in high-performance polymer-fullerene organic photovoltaic cells. *Nat Commun* **4**, 2867 (2013).
9. Shaw PE, Ruseckas A, Samuel IDW. Exciton diffusion measurements in poly(3-hexylthiophene). *Adv Mater* **20**, 3516–3520 (2008).
10. Markov DE, Tanase C, Blom PWM et al. Simultaneous enhancement of charge transport and exciton diffusion in poly (*p*-phenylene vinylene) derivatives. *Phys Rev B* **72**, 045217 (2005).
11. Lewis AJ, Ruseckas A, Gaudin OPM et al. Singlet exciton diffusion in MEH-PPV films studied by exciton–exciton annihilation.

Org Electron **7**, 452–456 (2006).
12. Balasubrahmaniyam M, Simkhovich A, Golombek A et al. From enhanced diffusion to ultrafast ballistic motion of hybrid light–matter excitations. *Nat Mater* **22**, 338–344 (2023).
13. Liu B, Huang XJ, Hou SC et al. Photocurrent generation following long-range propagation of organic exciton–polaritons. *Optica* **9**, 1029–1036 (2022).
14. Tichauer RH, Sokolovskii I, Groenhof G. Tuning the coherent propagation of organic exciton-polaritons through the cavity Q-factor. *Adv Sci* **10**, 2302650 (2023).
15. Haedler AT, Kreger K, Issac A et al. Long-range energy transport in single supramolecular nanofibres at room temperature. *Nature* **523**, 196–199 (2015).
16. Wittmann B, Wenzel FA, Wiesneth S et al. Enhancing long-range energy transport in supramolecular architectures by tailoring coherence properties. *J Am Chem Soc* **142**, 8323–8330 (2020).
17. Jin XH, Price MB, Finnegan JR et al. Long-range exciton transport in conjugated polymer nanofibers prepared by seeded growth. *Science* **360**, 897–900 (2018).
18. Wan Y, Stradomska A, Knoester J et al. Direct imaging of exciton transport in tubular porphyrin aggregates by ultrafast microscopy. *J Am Chem Soc* **139**, 7287–7293 (2017).
19. Caram JR, Doria S, Eisele DM et al. Room-temperature micron-scale exciton migration in a stabilized emissive molecular aggregate. *Nano Lett* **16**, 6808–6815 (2016).
20. Akselrod GM, Deotare PB, Thompson NJ et al. Visualization of exciton transport in ordered and disordered molecular solids. *Nat Commun* **5**, 3646 (2014).
21. Najafov H, Lee B, Zhou Q et al. Observation of long-range exciton diffusion in highly ordered organic semiconductors. *Nat Mater* **9**, 938–943 (2010).
22. Wan Y, Guo Z, Zhu T et al. Cooperative singlet and triplet exciton transport in tetracene crystals visualized by ultrafast microscopy. *Nat Chem* **7**, 785–792 (2015).
23. Ziegler JD, Zipfel J, Meisinger B et al. Fast and anomalous exciton diffusion in two-dimensional hybrid perovskites. *Nano Lett* **20**, 6674–6681 (2020).
24. Xiao X, Wu M, Ni ZY et al. Ultrafast exciton transport with a long diffusion length in layered perovskites with organic cation functionalization. *Adv Mater* **32**, 2004080 (2020).
25. Wagner K, Zipfel J, Rosati R et al. Nonclassical exciton diffusion in monolayer WSe_2. *Phys Rev Lett* **127**, 076801 (2021).
26. Mazzio KA, Luscombe CK. The future of organic photovoltaics. *Chem Soc Rev* **44**, 78–90 (2015).
27. Ding DX, Wang ZC, Duan CB et al. White fluorescent organic light-emitting diodes with 100% power conversion. *Research* **2022**, 0009 (2022).
28. Duan CB, Han CM, Zhang J et al. Manipulating charge-transfer excitons by exciplex matrix: toward thermally activated delayed fluorescence diodes with power efficiency beyond 110 lm W^{-1}. *Adv Funct Mater* **31**, 2102739 (2021).
29. Chow PCY, Someya T. Organic photodetectors for next‐generation wearable electronics. *Adv Mater* **32**, 1902045 (2020).
30. Liu K, Ouyang B, Guo XL et al. Advances in flexible organic field-effect transistors and their applications for flexible electronics. *npj Flex Electron* **6**, 1 (2022).
31. Dai ST, Li XZ, Liu JW et al. Conformation‐confined organic butterfly‐molecule with high photoluminescence efficiency, deep‐blue amplified spontaneous emission, and unique piezochromic luminescence. *Angew Chem Int Ed* **64**, e202414960 (2025);
32. Liu HP, Lu ZQ, Zhang ZL et al. Highly elastic organic crystals for flexible optical waveguides. *Angew Chem Int Ed Engl* **57**, 8448–8452 (2018).
33. Penzo E, Loiudice A, Barnard ES et al. Long-range exciton diffusion in two-dimensional assemblies of cesium lead bromide perovskite nanocrystals. *ACS Nano* **14**, 6999–7007 (2020).
34. Shi ZF, Ni YZ, Huang JS. Direct observation of fast carriers transport along out-of-plane direction in a Dion–Jacobson layered perovskite. *ACS Energy Lett* **7**, 984–987 (2022).
35. Li XZ, Aihemaiti N, Fang HH et al. Optical visualization of photoexcitation diffusion in all-inorganic perovskite at high temperature. *J Phys Chem Lett* **13**, 7645–7652 (2022).
36. Li ZD, Lu XB, Cordovilla Leon DF et al. Interlayer exciton transport in $MoSe_2/WSe_2$ heterostructures. *ACS Nano* **15**, 1539–1547 (2021).
37. Tagarelli F, Lopriore E, Erkensten D et al. Electrical control of hybrid exciton transport in a van der Waals heterostructure. *Nat Photonics* **17**, 615–621 (2023).
38. Sun Z, Ciarrocchi A, Tagarelli F et al. Excitonic transport driven by repulsive dipolar interaction in a van der Waals heterostructure. *Nat Photonics* **16**, 79–85 (2022).
39. deQuilettes DW, Brenes R, Laitz M et al. Impact of photon recycling, grain boundaries, and nonlinear recombination on energy transport in semiconductors. *ACS Photonics* **9**, 110–122 (2022).
40. An B, Li Z, Wang Z et al. Direct photo-oxidation of methane to methanol over a mono-iron hydroxyl site. *Nat Mater* **21**, 932–938 (2022).
41. Wang H, Yong DY, Chen SC et al. Oxygen-vacancy-mediated exciton dissociation in BiOBr for boosting charge-carrier-involved molecular oxygen activation. *J Am Chem Soc* **140**, 1760–1766 (2018).
42. Mateker WR, McGehee MD. Progress in understanding degradation mechanisms and improving stability in organic photovoltaics. *Adv Mater* **29**, 1603940 (2017).
43. He D, Zeng M, Zhang ZZ et al. Exciton diffusion and dissociation in organic and quantum-dot solar cells. *SmartMat* **4**, e1176 (2023).
44. Sajjad MT, Ruseckas A, Samuel IDW. Enhancing exciton diffusion length provides new opportunities for organic photovoltaics. *Matter* **3**, 341–354 (2020).
45. Sneyd AJ, Beljonne D, Rao A. A new frontier in exciton transport: transient delocalization. *J Phys Chem Lett* **13**, 6820–6830 (2022).
46. Lu T, Chen QX. Interaction region indicator: a simple real space function clearly revealing both chemical bonds and weak interactions. *Chem–Methods* **1**, 231–239 (2021).
47. Spackman PR, Turner MJ, McKinnon JJ et al. *CrystalExplorer*: a program for Hirshfeld surface analysis, visualization and quantitative analysis of molecular crystals. *J Appl Crystallogr* **54**, 1006–1011 (2021).
48. Janiak C. A critical account on π–π stacking in metal complexes with aromatic nitrogen-containing ligands. *J Chem Soc, Dalton Trans* 3885–3896 (2000).
49. Spackman MA. Molecules in crystals. *Phys Scr* **87**, 048103 (2013).
50. Dubin F, Melet R, Barisien T et al. Macroscopic coherence of a single exciton state in an organic quantum wire. *Nat Phys* **2**, 32–35 (2006).

51. Engel GS, Calhoun TR, Read EL et al. Evidence for wavelike energy transfer through quantum coherence in photosynthetic systems. *Nature* **446**, 782–786 (2007).
52. Cao JS, Cogdell RJ, Coker DF et al. Quantum biology revisited. *Sci Adv* **6**, eaaz4888 (2020).

Acknowledgements

The authors thank the National Natural Science Foundation of China (No. 62075115, 62335013, 22275065, 52073116), the National Key R&D Program of China (No. 2022YFB4600400), and the Natural Science Foundation of Jilin Province (20240101003JJ) for their financial support.

Author contributions

X.-Z. Li and S. T. Dai designed, fabricated, characterized the samples, and wrote the original manuscript. Y. W. Ren, Y. Yuan, and C.C. Zhang helped with the sample measurement. J. W. Liu and P. Wang helped with the characterization and analysis of crystal structures. F. X. Yang, W. J. Tian, B. Xu, H. H. Fang, and H. B. Sun conceived the idea and supervised the project. All authors contributed to the discussion and preparation of the manuscript.

Competing interests

The authors declare no competing financial interests.

Supplementary information

Supplementary information for this paper is available at https://doi.org/10.29026/oea.2025.240207

Scan for Article PDF